THE JOURNAL OF PHYSICAL CHEMISTRY C

Article

Cite This: J. Phys. Chem. C 2018, 122, 28265−28272

pubs.acs.org/JPCC

Ubiquitous Short-Range Distortion of Hybrid Perovskites and Hydrogen-Bonding Role: the $MAPbCl_3$ Case

Andrea Bernasconi,[†] Katharine Page,[‡] Zhenbang Dai,[§] Liang Z. Tan,[⊥] Andrew M. Rappe,[§] and Lorenzo Malavasi*[,†]

[†]Department of Chemistry and INSTM, Viale Taramelli 16, 27100, Pavia, Italy

[‡]Oak Ridge National Laboratory, Spallat Neutron Source, Oak Ridge, Tennessee, United States

[§]Department of Chemistry, University of Pennsylvania, Philadelphia, Pennsylvania, 19104-6323, United States

[⊥]The Molecular Foundry, Lawrence Berkeley National Laboratory, Berkeley, California 94720, United States

Supporting Information

ABSTRACT: The local structure of $MAPbCl_3$ has been investigated through the combined use of X-ray and neutron pair distribution function (PDF) analysis and computational modeling. The results indicate the presence of a significant level of distortion at the short-range, irrespective of the average structure found by diffraction, and this suggests a possible correlation between the type of distortion and the features of the strongest H−X bond. The distortion of the octahedra decreases by reducing temperature, but the overall tilting of the octahedral system increases, and such tilting depends on the size of the anion. The comparison of the short-range structural data available on the $MAPbX_3$ family strongly indicates a common pattern of the local structural distortion in these systems.

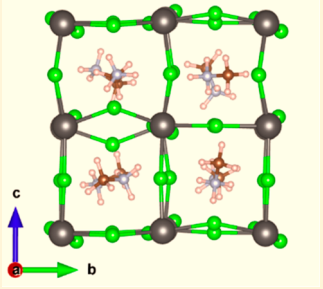

INTRODUCTION

Hybrid organic−inorganic perovskites (HOIPs) are fascinating materials, which prompted a very lively research activity in the field of materials science for their potential use in photovoltaics and light-emitting applications.[1−4] From a structural point of view, HOIPs share many similarities with the fully inorganic perovskites, but the presence of an organic cation on the A-site leads to a more complicated scenario at the microscopic level. In inorganic perovskites, only strong ionic or covalent bonding is present, while in hybrid perovskites, the organic A-cation (usually the methylammonium, MA, ion) gives rise to weak chemical interactions, in particular hydrogen bonding, with the surrounding halogen environment. In addition, the organic cation is involved in order−disorder transitions, being fully disordered in the cubic phase (*Pm*-3*m*) displayed by HOIPs at room temperature (or for MAPI above 330 K), being partially disordered in the tetragonal phase (*I*4/*mcm*), and being fully ordered in the low-*T* orthorhombic phase (*Pnma*).[5−7] There is growing evidence that the weak interactions (hydrogen bonding) between the organic cation and the halogens induce local distortions to the PbX_6 octahedra, which are at the basis of the superior optoelectronic properties of these systems and which could be related to the enhanced suppression of charge-carrier recombination.[8−10] Most of the experimental results available can locally probe the dynamics and orientation of the molecular part of the HOIPs (spectroscopically), but they lack reliable correlations with the inorganic framework features, which are usually (indirectly) determined by spatially averaged probes such as X-ray or neutron diffraction. Concerning the latter, most of the neutron-based studies did not make use of deuterated samples to eliminate the incoherent scattering coming from hydrogen. With standard average structure probes, the motion of the organic cation in the high symmetry phases of HOIPs prevented a structural insight into the actual interactions between the organic cation and the inorganic part, which has been possibly only for the ordered orthorhombic phases of $MAPbX_3$ at very low temperatures (X = Cl, Br, and I).[11,12]

While there is a general consensus on the presence and impact of local distortions in HOIPs, clear experimental evidence of such phenomena is scarce, and the few experimental findings around this topic resulted from the application of short-range-ordered structural probes such as neutron (on deuterated samples) and X-ray pair distribution function (PDF) analysis. These were applied to the $MAPbI_3$ and $MAPbBr_3$ systems, and a general conclusion deriving from them is the clear evidence of a distorted local structure (in particular, orthorhombic) irrespective of the actual average structure (cubic, tetragonal, or orthorhombic), which dominates at short distances (typically below 10 Å). Above this distance, the average and local structures tend to reconcile each other.[5,13−16]

To complete the description of the local structure of HOIPs and to provide a unifying view of the local structure of MA-based hybrid perovskites, in this paper, we present the results of temperature-variable NPDF (neutron PDF; data collected at 300, 225, 175, 150, 100, 50, and 5 K) and X-ray PDF (data collected at 373, 300, 250, 200, and 100 K) studies on the

Received: October 16, 2018
Revised: November 21, 2018
Published: November 26, 2018

DOI: 10.1021/acs.jpcc.8b10086
J. Phys. Chem. C 2018, 122, 28265−28272

$MAPbCl_3$ system, as well as a comparison with the PDF of $MAPbBr_3$ in order to unveil some common features.

METHODS

Sample Preparation. Deuterated sample of formula $MAPbCl_3$ has been prepared starting from a proper amount of Pb acetate dissolved in an excess of DCl (Aldrich, 47 wt % in D_2O, 99% atom % D) under nitrogen atmosphere and stirring. The solution is heated to 100 °C, and a solution of CD_3ND_2 (Aldrich, 99 atom % D) is added in equimolar amount. A precipitate is formed immediately after the amine addition. The solution is then cooled to 46 °C at 1 °C/min, and the precipitate is immediately filtered and dried under vacuum overnight.[17]

High-Energy X-ray Diffraction Measurements. The data were collected at the ID11 Material Science beamline of the European Synchrotron Radiation Facility (ESRF, Grenoble). A monochromatic high flux beam with an energy corresponding to the Pt K edge (λ = 0.158135 Å) and a size of 200 × 200 μm was used to perform a transmission diffraction experiment.[18] Sample powder was loaded into a 1 mm diameter borosilicate-glass capillary. The 2D detector (ESRF, Frelon camera) was placed at 44 cm from the sample for high-resolution data (suitable for Rietveld refinement, Q_{MAX} = 8.3 Å^{-1}) and at 9.5 cm from the sample for the near-field configuration (suitable for PDF analysis, Q_{MAX} = 30.1 Å^{-1}). For the high-resolution data, five images with an exposure time of 1 s/image have been collected for each investigated temperature. For the near-field data, 1500 images with an exposure time of 0.5 s were collected for each investigated temperature. This large number of images was selected to improve the counting statistic, especially in the high-Q region, which is particularly important for total scattering experiments. Moreover, for the near-field measurements, the empty capillary was measured as well with the same counting statistic. A nitrogen cryostream (Oxford Cryostream 600) was placed laterally with respect to the sample to cover the 100−373 K temperature range. Images (for both configurations) were normalized for the incident flux and then were azimuthally integrated by using pyFAI software.[19] At this point, high-resolution data were processed by Rietveld refinement using Fullprof software.[20] The methylammonium group was included in the refinement, but the coordinates were kept fixed, and the isotropic thermal displacement parameter was kept fixed at 0.025 Å^2. Near-field data were first processed by PDFgetX3 to get first the total scattering function $S(Q)$ by

$$S(Q) = \frac{I_C - \langle f(Q)^2\rangle + \langle f(Q)\rangle^2}{\langle f(Q)\rangle^2}$$

where I_C is the coherent intensity and $f(Q)$ is the average X-ray atomic form factor of the sample.[21] This function is then sine Fourier transformed to get the reduced PDF $G(r)$ following

$$G(r) = \frac{2}{\pi}\int_0^\infty Q[S(Q) - 1]\sin(Qr)dQ$$

At this level, real-space modeling was performed by means of the PDFgui program.[22] For each temperature, scale factor, cell parameters, and isotropic thermal displacement parameters were refined. In the case of tetragonal (space group) and orthorhombic (space group) chloride atoms, coordinates were also refined according to symmetry constraints. Experimental resolution parameters known as Q_{DAMP} and Q_{BROAD} were determined on a CeO_2 standard material measured at the same conditions, resulting in 0.0244 and 0.0296, respectively. The methylammonium group was included in the refinement (atomic position kept fixed). No correlation larger than 0.8 in the orthorhombic fit was observed. The effect of the Q range on the extracted $G(r)$ values has even been evaluated by cutting the data at 23 Å^{-1}, at the expense of real-space resolution but with the benefit that possible high-Q bias components (statistical noise and Compton scattering overall) are minimized.

Neutron Total Scattering Data Collection and Analysis. Neutron powder diffraction (NPD) measurements at 5, 50, 100, 150, 175, 225, and 300 K were carried out on the NOMAD diffractometer at the Oak Ridge Laboratories. The samples were loaded into vanadium cans and were measured in an orange cryostat outfitted with vanadium tails. Empty sample environment, empty vanadium can, and vanadium rod data were collected for background and normalization corrections. The corrected total scattering structure function, $S(Q)$, was calculated with the NOMAD data reduction software, and the PDF was obtained by Fourier transformation of $S(Q)$.[23] A Q_{max} = 31 Å^{-1} was used. An analogous strategy was used for fitting the data (by means of PDFGui) where N and C atoms were kept fixed while refining the D atoms position and Biso in order to reduce the number of parameters. Attempts to refine as well the N and C, however, did not lead to significant improvements in the fits while indicating some correlations greater than 0.8.

RESULTS AND DISCUSSION

Figure 1 reports the NPDFs and X-ray PDFs for $MAPbCl_3$ as a function of temperature in the 1−10 Å range.

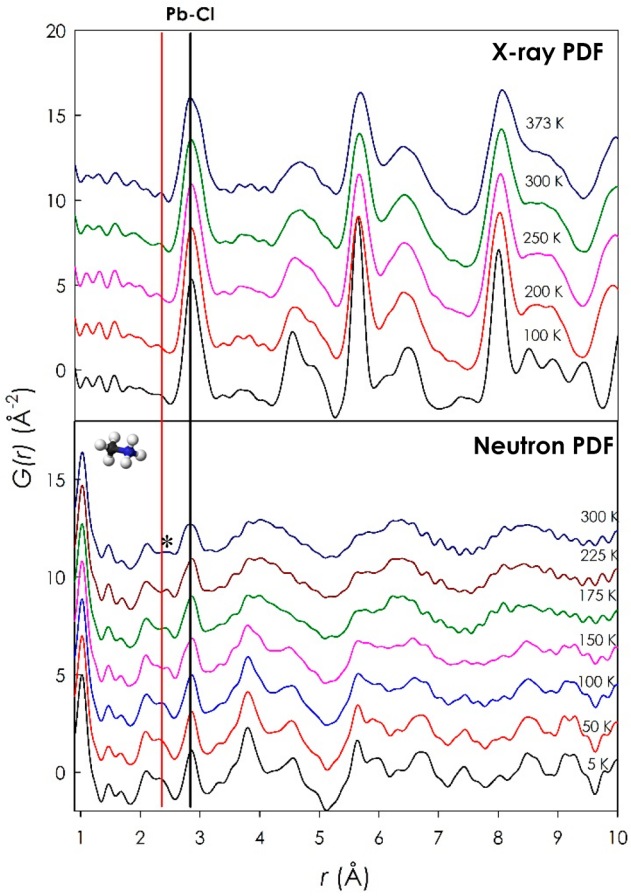

Figure 1. X-ray (top panel) and neutron (bottom panel) PDFs for $MAPbCl_3$ as a function of temperature.

DOI: 10.1021/acs.jpcc.8b10086
J. Phys. Chem. C 2018, 122, 28265−28272

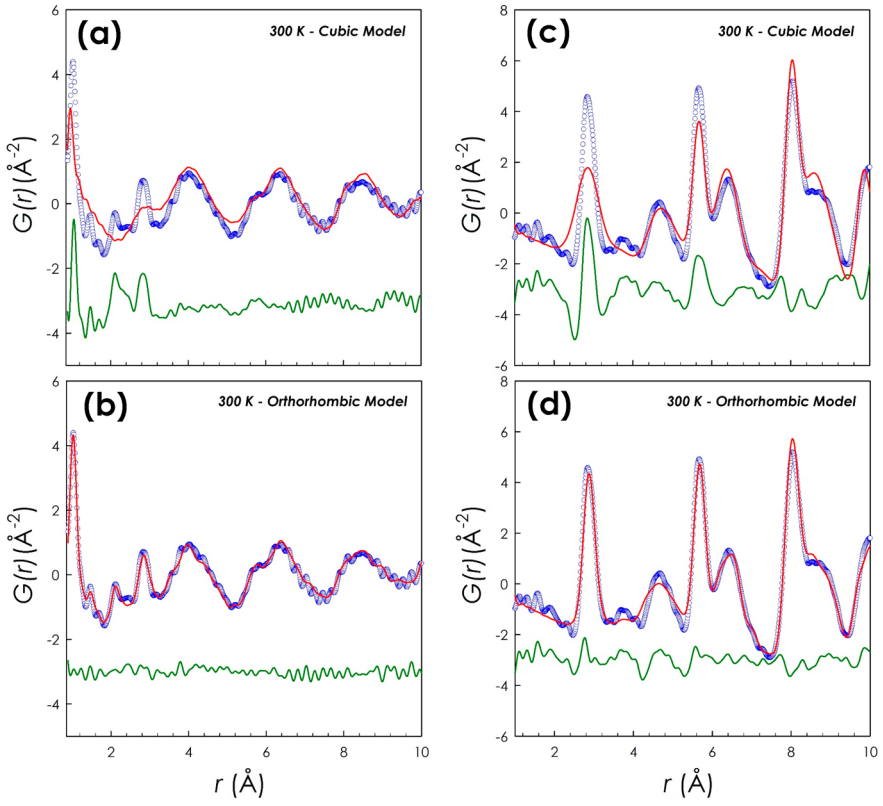

Figure 2. Refinement of 300 K neutron PDF of $MAPbCl_3$ versus (a) the cubic (*Pm*-3*m*) model and (b) the orthorhombic (*Pnma*) model; refinement of the 300 K X-ray PDF of $MAPbCl_3$ versus (c) the cubic (*Pm*-3*m*) model and (d) the orthorhombic (*Pnma*) model. Blue open circles, experimental data; red line, calculated; green line, difference (shifted by −3 for ease of visualization).

The X-ray PDF is sensitive only to heavy atoms and is dominated by Pb and Cl bond pairs, with the first peak appearing around 3 Å (i.e., Pb−Cl octahedra bond pairs). By a simple visual inspection of the top panel of Figure 1, it is possible to observe significant similarities between the data collected between 373 and 200 K, while at 100 K, more distinct features are present (see, for example, the peaks between 4.5 and 5 Å and those between 8 and 9 Å which become more resolved at this temperature) together with a general peak sharpening. On the other hand, neutron PDF (bottom panel, Figure 1) is highly sensitive to light atoms and, in particular, to hydrogen (deuterium in the present samples), thus allowing a closer look to the organic component (i.e., methylammonium). At first glance, the neutron PDFs resemble each other at all temperatures in the low *r*-range (below 3 Å), analogously to our previous observation for the $MAPbBr_3$ system.[14] The red line in Figure 1 marks the upper limit of the region pertaining to the intramolecular bond pairs of the MA cation (peaks up to about 2.1 Å), which are not affected by the temperature or crystal structure change. Such a result was *indirectly* suggested by QENS (quasi-elastic neutron scattering) data on $MAPbI_3$, indicating no major changes to the characteristics of the MA group through the crystal structure transitions despite the structural changes observed in the neutron diffraction patterns (i.e., an average probe).[6] $MAPbCl_3$ has two structural phase transitions from the cubic phase (*Pm*-3*m*), stable at room temperature, to the orthorhombic phase (*Pnma*), below about 170 K, passing through the tetragonal phase (*P*4/*mmm*).[24] On the other hand, at higher *r*, the NPDFs show a significant thermal broadening up to about 175 K. Another interesting characteristic of the NPDFs (bottom panel of Figure 1) is the first peak corresponding to the shortest D−Cl bond (marked with an asterisk). This occurs around 2.5 Å for data between 300 and 150 K, contracting for scans between 100 and 5 K. This H−X bond corresponds to the interaction between the hydrogen atoms of the amino group and the halogen and is considered to be due to the strongest hydrogen bonding as a consequence of the electronegativity of nitrogen (with respect to the hydrogen atoms of the $-CH_3$ group). Up to now, structural information on this bond has been obtained theoretically or experimentally only by means of very low-*T* neutron diffraction (i.e., in the orthorhombic phase) where the organic group reorientation is quenched.[11,12] This is due to the difficulty of clearly defining the structural features of the MA component in the cubic and tetragonal phases, because these cations move between different orientations, but only the static (time-averaged) structural features are probed by average structure tools such as diffraction. This dynamic component of the hydrogen bonding is expected to strongly affect the local distortion of the Pb−halide octahedra and may give rise to distinct patterns in the local structure of the MA perovskite systems.[25,26]

To further investigate the local structure and distortion of $MAPbCl_3$, we analyzed the X-ray and neutron PDFs, starting with the 300 K structure, by checking the validity of the average structure proposed at this temperature, that is, the *Pm*-3*m* cubic structure.[24]

Figure 2 reports the refinements of the X-ray and neutron PDFs in the 1−10 Å range for $MAPbCl_3$ collected at 300 K against the cubic average structure and the orthorhombic structure (*Pnma*).

It is clear, by simple visual inspection, that the proposed cubic model obtained from X-ray and neutron diffraction is not suited

DOI: 10.1021/acs.jpcc.8b10086
J. Phys. Chem. C 2018, 122, 28265−28272

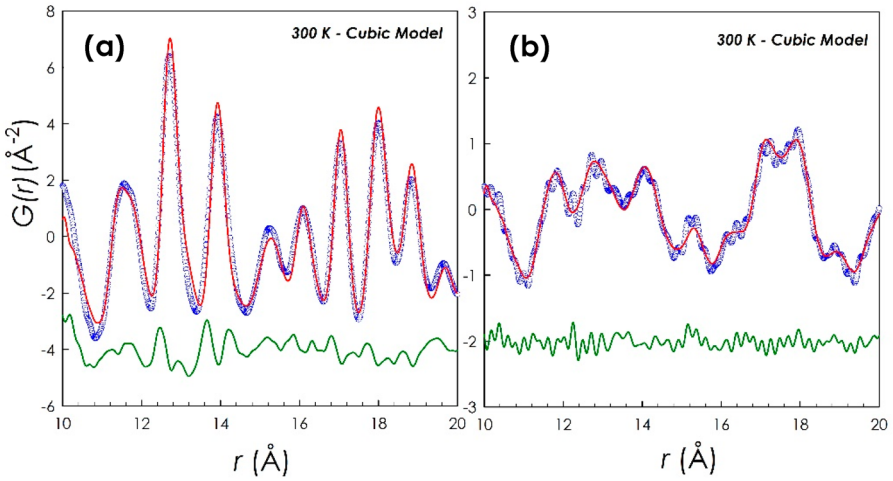

Figure 3. (a) Refinement of 300 K X-ray PDF of $MAPbCl_3$ against the cubic (*Pm*-3*m*) model and (b) refinement of the 300 K neutron PDF of $MAPbCl_3$ against the cubic (*Pm*-3*m*) model in the 10−20 Å range. Blue open circles, experimental data; red line, calculated; green line, difference (shifted by −3 for ease of visualization).

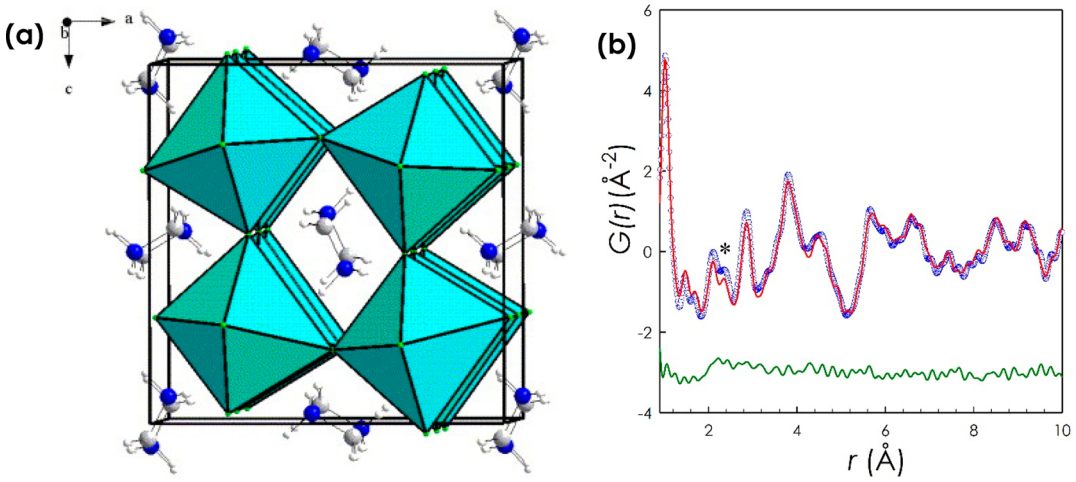

Figure 4. (a) View of the ordered phase of methylammonium lead chloride along *b*. Two MA cations reside in the *ac* plane (taken from ref 12). (b) Refinement of 100 K NPDF of $MAPbCl_3$ against the orthorhombic model with doubled unit cell (*Pnma*). Blue empty circles, experimental data; red line, calculated; green line, difference (shifted by −3 for ease of visualization).

to describe the local structure of $MAPbCl_3$ at 300 K, while a more distorted local structure (orthorhombic) is required to capture both the features dominated by light atoms and heavy atoms. Agreement factors (R_{wp}) are 14.9% (neutron) and 17.8% (X-ray) for the orthorhombic model and 52% (neutron) and 35% (X-ray) for the cubic model. These results agree with previous studies on $MAPbI_3$ and $MAPbBr_3$.[13−15]

This first piece of evidence is of key importance in the current research because it extends the actual knowledge on the local distortions of hybrid perovskites, confirming that *all* the members of the $MAPbX_3$ family present a significant degree of distortion, at room temperature, at the local scale. In addition, for those systems where NPDF data are available (which can probe the organic component of the PDF), that is, $MAPbBr_3$ and $MAPbCl_3$, it is confirmed that the distortion observed is compatible with an orthorhombic local symmetry (*Pnma*). Such local structure works well for the NPDF data up to 150 K and for the X-ray PDF up to 200 K for $MAPbCl_3$. Figure 1 of the Supporting Information (SI) reports, by way of example, the NPDF data at 150 K and the X-ray PDF data at 200 K fitted against the *Pnma* structure. For this whole set of NPDF data (150 K ≤ *T* ≤ 300 K), the same local structure works well, and all these data have an analogous D−Cl bond distance around 2.5 Å, suggesting that this hydrogen bond plays a role in stabilizing this local structure.

It is, however, of further interest to observe that a reconciliation between the average structures (as determined by Rietveld refinement) and the PDF data usually occurs if the data fit is performed starting from 10 Å, that is, moving away from the short-range scale. Figure 3 shows the NPDF and X-ray PDFs at 300 K in the 10−20 Å range for $MAPbCl_3$ fitted against the symmetry obtained by Rietveld refinement (i.e., cubic).

In both cases, the cubic structure nicely describes the PDFs (no significant improvement in the R_{wp} is observed by applying the *Pnma* model to this *r* range), and the lattice parameter determined is in fairly good agreement with the one obtained from Rietveld refinement, that is, 5.6803(6) Å (Rietveld), 5.6818(4) Å (X-ray PDF), and 5.675(9) Å (NPDF). A full set of Rietveld refinement results of the X-ray diffraction data as a function of temperature are reported in Table 1 and Figure 2 of the SI.

DOI: 10.1021/acs.jpcc.8b10086
J. Phys. Chem. C 2018, 122, 28265−28272

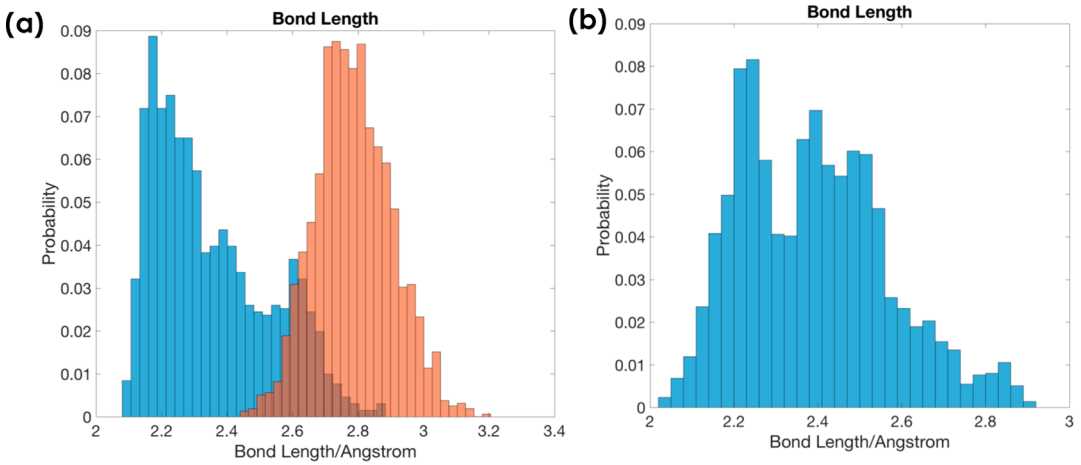

Figure 5. (a) Distribution of hydrogen-bonding lengths for amino group hydrogens (blue) and methyl group hydrogens (orange) for low temperatures. (b) Distribution of hydrogen-bonding lengths for amino group hydrogens at room temperature.

As mentioned previously, the cubic *Pm-3m* structure together with local *Pnma* distortions works well for a wide range of temperatures, namely, down to about 150 K, in describing the local structure of $MAPbCl_3$. However, the data below this temperature present structural features which cannot be properly described by the unit cell used above this range. As a matter of fact, Chin et al. showed, through X-ray and neutron diffraction on a sample of $CH_3ND_3PbCl_3$, that at 80 K (the minimum fixed temperature in their work), each of the orthorhombic axes is doubled, resulting in *Pnma* symmetry.[12] This result is confirmed by Rietveld refinement of the synchrotron X-ray diffraction data on $MAPbCl_3$ at 100 K (Figure 3 and Table 2 of the SI), thus indicating, thanks to the variable temperature data collected in the present work, that such unit cell doubling occurs between 150 and 100 K. By making use of this model structure, represented in Figure 4a, we fitted the NPDF data at 100 K, and the result is presented in Figure 4b.[12]

The fit results are reported in Table 2 of the SI. The agreement factor of this fit was 14.2% without significant parameter correlations. Such a result confirms the reconciliation between the average and local structure when the MA group is locked in fixed positions, as it occurs for the low-*T* orthorhombic structures.[11,12] Another interesting result coming from this analysis is that the shortest D−Cl bond distance is now around 2.25 Å (marked with an asterisk in Figure 4) without significant variations for the NPDF data at 50 and 5 K. Such distances have also been confirmed by computational modeling which indicates the low-energy positions of the MA group within the framework created in the crystal structure.

To investigate the local structure of $MAPbCl_3$ theoretically, we start by constructing a database of $MAPbCl_3$ with 50 different structural configurations. In each configuration, we initialize the orientation of the organic molecules with some random directions and then fully relax the system to a local minimum, allowing for change of cell parameters. Such a procedure mimics high-temperature structural fluctuations away from low-energy configurations. All the structures in this database are constructed in a 2 × 2 × 2 supercell. The calculations are performed via density functional theory (DFT) with the PBE exchange-correlation energy functional, including the Grimme-D2 van der Waals correction, using the QUANTUM-ESPRESSO code.[27−29] The plane-wave energy cutoff is chosen to be 50 Ry, and a 4 × 4 × 4 k-grid is used. We used norm-conserving pseudopotentials constructed using the RRKJ method and with the OPIUM pseudopotential generator.[30,31]

In Figure 5a, we show that although the hydrogen-bonding (for hydrogen atoms in amine groups) lengths may vary for different configurations, they are skewed toward shorter bond lengths and are peaked at 2.2 Å, consistent with the experimental results reported earlier for low temperatures. We find that the average bond length over the entire database is 2.35 Å. Also, we find that the hydrogen-bonding length for hydrogen atoms in methyl groups is centered around 2.8 Å because of the weaker bonding strength of methyl group hydrogen atoms.

To simulate the situation of high temperature, we perform a Born−Oppenheimer ab initio molecular dynamics simulation at 300 K with the experimental lattice parameters.[32] To ensure consistency, we chose the same pseudopotentials and van der Waals correction as we used for the previous relaxation calculation. We use an Anderson thermostat with the tolerance of the fluctuation to be 10 K.[33] After equilibration, we sample the hydrogen-bond lengths of 200 snapshots. In Figure 5b, we show that the distribution becomes broader, and the bond length distribution is centered at 2.45 Å, which indicates that temperature significantly influences the hydrogen-bonding length.

At this point, we can summarize some of the key results:

(1) The local structure of cubic $MAPbCl_3$ (*T* range between 373 and 150 K) is described by means of an orthorhombic symmetry (namely, *Pnma*).
(2) Reconciliation with the average structure occurs for $r > 10$ Å.
(3) Below 150 K, the local structure and the average structures are analogous and characterized by an orthorhombic doubled unit cell with space group *Pnma*.
(4) The shortest D−Cl bond moves from around 2.5 Å between 300 and 150 K to 2.25 Å (data from 100 K).

Finally, to gain further insight into the variation of the local structure as a function of temperature, we analyzed the distortion of the $PbCl_6$ octahedra. Such data have been mainly derived from X-ray PDF analysis, being more sensitive to the heavy atoms and because the scattering cross sections of Pb and Cl for neutrons are similar. The trend of Pb−Cl bond lengths as a function of temperature (as determined from X-ray PDF) is reported in Figure 4 of the SI. For data up to 200 K (described by a single unit cell in the *Pnma* space group), there is a general

DOI: 10.1021/acs.jpcc.8b10086
J. Phys. Chem. C 2018, 122, 28265−28272

contraction of Pb−Cl distances by lowering the temperature and a tendency to reduce the difference between the three Pb−Cl distances. This is in agreement as well with the reduction in the relative difference between the three orthorhombic lattice parameters (obtained from X-ray PDF in the 1−10 Å, Figure 5 of the SI) by decreasing *T*, indicating that the Pb−Cl octahedra become more distorted by increasing temperature, analogously to the results obtained for $MAPbBr_3$.[14] In the present discussion, we refer, however, to the Φ parameter defining the overall tilting degree of the octahedra, expressed in terms of the individual tilt angles along the three pseudocubic axes of the orthorhombic structure (for more details, see ref 34).[34] This information is of great significance in particular when coupled to the bond-length trend of the single octahedra and gives a more quantitative representation of the overall distortion within the perovskite framework. Figure 6 reports the trend of the tilting parameters as

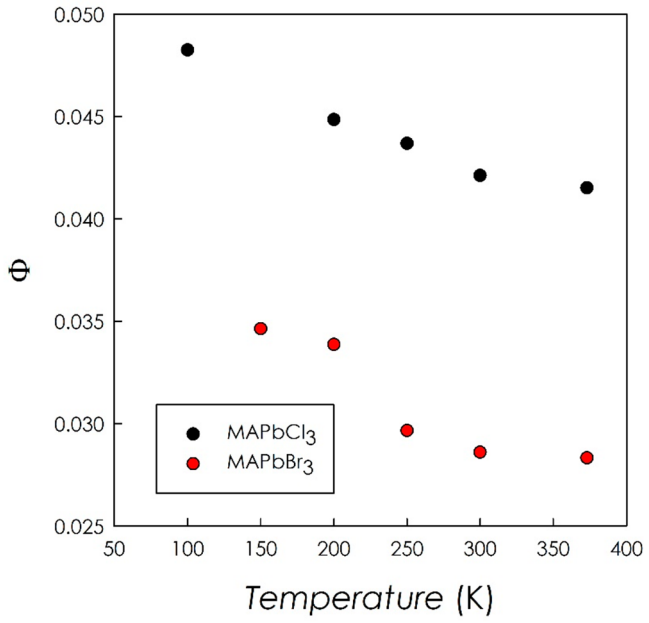

Figure 6. Tilting parameter Φ as a function of temperature for $MAPbCl_3$ and $MAPbBr_3$ as determined form the analysis of the local structure by means of X-ray PDF.

a function of temperature for $MAPbCl_3$ together with the data for $MAPbBr_3$, obtained in the same way, i.e., from the fit of the local orthorhombic structure of the 1−10 Å X-ray PDFs.[14]

Figure 6 shows that the overall tilting of the octahedra increases by reducing temperature even though the single octahedra become less distorted for both systems by lowering *T* (present results and ref 13). Unfortunately, at present, PDF data of the same quality as the present ones are not available for $MAPbI_3$, but we may expect that by increasing the volume of the PbI_6 octahedra the overall tilt will further decrease according to the observation in ref 35. The interesting feature of defining the tilting of the perovskite systems lies in the possible search for ferroelectricity in hybrid perovskites. As a matter of fact, this has been theoretically correlated to the presence of local distortion in $MAPbI_3$ and has been postulated that this tendency could be further enhanced by reducing the anion size, which may couple to the increased local tilting reported in the present work. Such an aspect is worth being further analyzed experimentally and computationally thanks to the data reported in the present work. However, we may expect that the averaging, at high temperatures, over dynamic differently oriented domains will result in a zero polarization of the whole system, and so, experimental studies with local probes would be of interest.[36]

Finally, a further conclusion we may draw from the present NPDF data on $MAPbCl_3$ and the data on $MAPbBr_3$ (taken from ref 14) is related to the hydrogen bonding of the first, strong D−X bond pair. In the data presented in this work, we have shown that, when the local structure can be modeled with the single *Pnma* unit cell, the length of this bond is constant and close to 2.5 Å. Of significant interest, for the $MAPbBr_3$ system, the position of this bond is analogous, as shown in Figure 7.

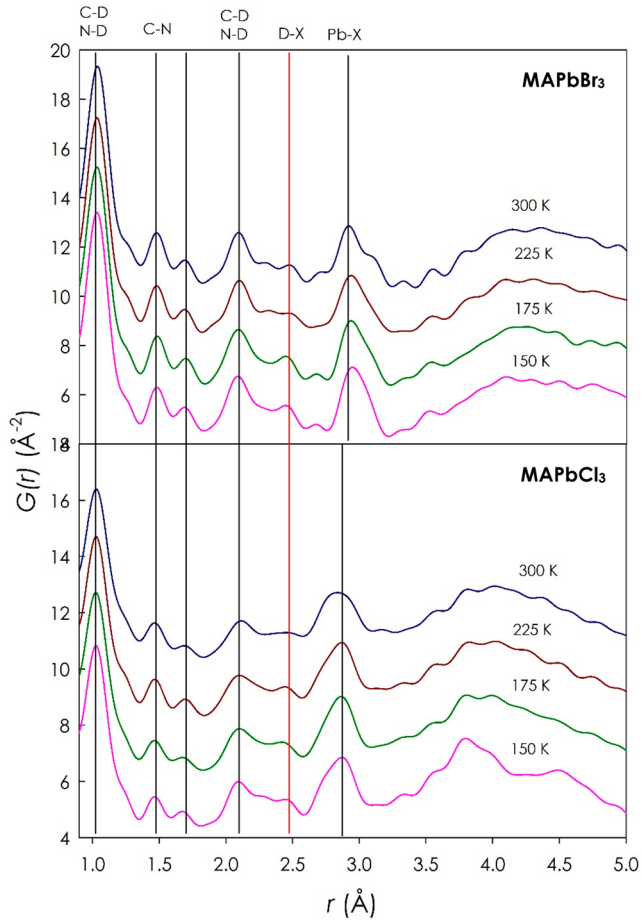

Figure 7. Neutron PDFs for (top panel) $MAPbBr_3$ and (bottom panel) $MAPbCl_3$ as a function of temperature. Vertical bars refer to specific bond pairs.

As can be seen, in addition, and more interestingly with respect to the similarity between the NPDFs for the $MAPbCl_3$ as a function of temperature (reported and discussed earlier), an impressive similarity is found and preserved in the low *r* range across the *two* systems, namely, $MAPbBr_3$ and $MAPbCl_3$. In Figure 7 are reported vertical bars corresponding to peculiar peaks found in the NPDFs of the two hybrid perovskites, which are related to the bond pairs denoted at the top of the figure. Pairs up to about 2.1 Å pertain to intramolecular pairs of the methylammonium cation which, as can be seen, do not shift because of symmetry reasons and as a function of the nature of the inorganic cage where they are found. We would like to focus the attention specifically on one peculiar peak of the NPDFs of Figure 7, namely, the peak corresponding to the H−X bond pair located at about 2.5 Å (vertical red line). As can be seen and

DOI: 10.1021/acs.jpcc.8b10086
J. Phys. Chem. C 2018, 122, 28265−28272

as already discussed, the position of this peak, and thus the bond length, never shifts by changing the temperature for both $MAPbBr_3$ and $MAPbCl_3$ (in the T range where they have the same unit cell at the local scale) and, surprisingly, does not appreciably move by passing from one HOIP to the other. This was suggested in a theoretical paper on $MAPbI_3$ where the authors noticed that in tetragonal and cubic crystal structures, the NH_3 component bonded strongly to I atoms with I−H bond lengths of about ≈2.6 Å and with no significant change in this I−H bond length by changing the lattice constants.[36] Of course, while the lengths are analogous between the two systems, the polarizability of the anion tends to increase with the size which in turn may correlate with a reduced overall tilting of the octahedra systems (Figure 5) and with the observed changes in the optical properties by changing the anion.[37] Clearly, the whole set of data presented for $MAPbBr_3$ and $MAPbCl_3$ suggests a correlation between the actual length of the D−X bond and the distortion observed at the local scale thanks to the NPDF data. There is strong evidence that the interaction between the MA group and the halogen dictates the symmetry of the local distortion which may, however, give origin to a different tilting patterns depending on the polarizability of the anion. On the basis of the present results, it would be of great importance to extend the actual approach to other systems containing different organic cations which were shown to lead to the formation of multiple hydrogen bonding (such as guanidinium) in order to establish an even more general correlation between such microscopic interactions and the local/average structures.[38]

CONCLUSIONS

In this work, we presented a detailed analysis of variable temperature X-ray and neutron PDF data for $MAPbCl_3$. Overall, the results obtained confirm the presence of an orthorhombic distortion at the local scale (1−10 Å) in analogy with Br- and I-based counterparts and that a reconciliation with the average structure determined from diffraction occurs above 10 Å. Such evidence indicates the ubiquitous nature of local distortion in lead-based hybrid perovskites. In addition, the comparison between the neutron PDF data available for $MAPbCl_3$ and $MAPbBr_3$ suggests a common pattern of the short-range distortion (orthorhombic, *Pnma*), which seems to be correlated to the strongest H−X bond found in these systems. An analysis of the local octahedral distortion through X-ray PDF indicates that the distortion of the single octahedra decreases by reducing the temperature, but at the same time, the tilting of the octahedral system increases, and such tilting increases by reducing the size of the anion. The set of data reported in this paper, together with the available information at the local scale on other lead-based hybrid perovskites, allows us to define the complete structural features of $MAPbX_3$ materials including the short-range order, thus providing a unique set of experimental data which represents a solid base to understand and further investigate the correlation between the opto-electronic properties and the structural properties in these fascinating systems.

ASSOCIATED CONTENT

Supporting Information

The Supporting Information is available free of charge on the ACS Publications website at DOI: 10.1021/acs.jpcc.8b10086.

Material synthesis and results of refinements and further experimental details (PDF)

AUTHOR INFORMATION

Corresponding Author

*E-mail: lorenzo.malavasi@unipv.it.

ORCID

Andrea Bernasconi: 0000-0002-9667-6798
Katharine Page: 0000-0002-9071-3383
Andrew M. Rappe: 0000-0003-4620-6496
Lorenzo Malavasi: 0000-0003-4724-2376

Notes

The authors declare no competing financial interest.

ACKNOWLEDGMENTS

The authors gratefully acknowledge the project PERSEO-"PERrovskite-based Solar cells: towards high Efficiency and lOng-term stability" (Bando PRIN 2015-Italian Ministry of University and Scientific Research (MIUR) Decreto Direttoriale 4 novembre 2015 n. 2488, project number 20155LECAJ) for funding. Z. D. acknowledges the support of the Office of Naval Research, under grant N00014-17-1-2574. A. M. R. acknowledges the support the National Science Foundation, under grant DMR-1719353. Z. D. and A. M. R. acknowledge computational support from the HPCMO of the US DoD. L. Z. T. acknowledges support from the Molecular Foundry at Lawrence Berkeley National Laboratory, supported by the Office of Science, Office of Basic Energy Sciences, of the U.S. Department of Energy under contract No. DE-AC02-05CH11231.

REFERENCES

(1) Zarick, H. F.; Soetan, N.; Erwin, W. R.; Bardhan, R. Mixed Halide Hybrid Perovskites: a Paradigm Shift in Photovoltaics. *J. Mater. Chem. A* **2018**, *6*, 5507−5537.

(2) Li, W.; Wang, Z.; Deschler, F.; Gao, S.; Friend, R. H.; Cheetham, A. K. Chemically Diverse and Multifunctional Hybrid Organic−inorganic Perovskites. *Nature Reviews Materials* **2017**, *2*, 16099.

(3) Stranks, S. D.; Snaith, H. J. Metal-halide Perovskites for Photovoltaic and Light-emitting Devices. *Nat. Nanotechnol.* **2015**, *10*, 391−402.

(4) Huang, J.; Yuan, Y.; Shao, Y.; Yan, Y. Understanding the Physical Properties of Hybrid Perovskites for Photovoltaic Applications. *Nature Reviews Materials* **2017**, *2*, 17042.

(5) Whitfield, P. S.; Herron, N.; Guise, W. E.; Page, K.; Cheng, Y. Q.; Milas, I.; Crawford, M. K. Structures, Phase Transitions and Tricritical Behavior of the Hybrid Perovskite Methyl Ammonium Lead Iodide. *Sci. Rep.* **2016**, *6*, 35658.

(6) Leguy, A. M. A.; Frost, J. M.A; McMahon, P.; Sakai, V. G.; Kockelmann, W.; Law, C.; Foglia, F.; Walsh, A.; O'Regan, B. C.; Nelson, J.; Cabral, J. T.; Barnes, P. R. F. The Dynamics of Methylammonium Ions in Hybrid Organic−inorganic Perovskite Solar Cells. *Nat. Commun.* **2015**, *6*, 7124.

(7) Weller, M. T.; Weber, O.; Henry, P. F.; Di Pumpo, A. M.; Hansen, T. C. Complete Structure and Cation Orientation in the Perovskite Photovoltaic Methylammonium Lead Iodide Between 100 and 352 K. *Chem. Commun.* **2015**, *51*, 4180−4183.

(8) Lee, J.-H.; Bristowe, N. C.; Lee, J. H.; Lee, S.-H.; Bristowe, P. D.; Cheetham, A. K.; Jang, H. M. Resolving the Physical Origin of Octahedral Tilting in Halide Perovskites. *Chem. Mater.* **2016**, *28*, 4259−4266.

(9) Ambrosio, F.; Wilktor, J.; De Angelis, F.; Pasquarello, A. Origin of Low Electron−hole Recombination Rate in Metal Halide Perovskites. *Energy Environ. Sci.* **2018**, *11*, 101−105.

(10) Motta, C.; El-Mellouhi, F.; Kais, S.; Tabet, N.; Alharbi, F.; Sanvito, S. Revealing the Role of Organic Cations in Hybrid Halide Perovskite $CH_3NH_3PbI_3$. *Nat. Commun.* **2015**, *6*, 7026.

DOI: 10.1021/acs.jpcc.8b10086
J. Phys. Chem. C 2018, 122, 28265−28272

(11) Swainson, I. P.; Hammond, R. P.; Soulliere, C.; Knop, O.; Massa, W. Phase Transitions in the Perovskite Methylammonium Lead Bromide, $CH_3ND_3PbBr_3$. *J. Solid State Chem.* **2003**, *176*, 97−104.
(12) Chi, L.; Swainson, I.; Cranswick, L.; Her, J.-H.; Stephens, P.; Knop, O. The Ordered Phase of Methylammonium Lead Chloride $CH_3ND_3PbCl_3$. *J. Solid State Chem.* **2005**, *178*, 1376−1385.
(13) Bernasconi, A.; Malavasi, L. Direct Evidence of Permanent Octahedra Distortion in $MAPbBr_3$ Hybrid Perovskite. *ACS Energy Lett.* **2017**, *2*, 863−868.
(14) Page, K.; Siewenie, L.; Quadrelli, P.; Malavasi, L. Short-Range Order of Methylammonium and Persistence of Distortion at the Local Scale in $MAPbBr_3$ Hybrid Perovskite. *Angew. Chem., Int. Ed.* **2016**, *55*, 14320−14324.
(15) Beecher, A.; Semonin, O.; Skelton, J.; Frost, J.; Terban, M.; Zhai, H.; Alatas, A.; Owen, J.; Walsh, A.; Billinge, S. Direct Observation of Dynamic Symmetry Breaking above Room Temperature in Methylammonium Lead Iodide Perovskite. *ACS Energy Lett.* **2016**, *1*, 880−887.
(16) Yaffe, O.; Guo, Y.; Tan, L. Z.; Egger, D. A.; Hull, T.; Stoumpos, C. C.; Zheng, F.; Heinz, T. F.; Kronik, L.; Kanatzidis, M. G.; Owen, J. S.; Rappe, A. M.; Pimenta, M. A.; Brus, L. E. Local Polar Fluctuations in Lead Halide Perovskite Crystals. *Phys. Rev. Lett.* **2017**, *118*, 136001.
(17) Mancini, A.; Quadrelli, P.; Amoroso, G.; Milanese, C.; Boiocchi, M.; Sironi, A.; Patrini, M.; Guizzetti, G.; Malavasi, L. Synthesis, Structural and Optical Characterization of $APbX_3$ (A = Methylammonium, Dimethylammonium, Trimethylammonium; X = I, Br,Cl) Hybrid Organic-inorganic Materials. *J. Solid State Chem.* **2016**, *240*, 55−60.
(18) Bernasconi, A.; Wright, J.; Harker, N. Total Scattering Experiments on Glass and Crystalline Samples at the ESRF on the ID11 Beamline. *Powder Diffr.* **2015**, *30*, S2−S8.
(19) Kieffer, J.; Wright, J. PyFAI: a Python Library for High Performance Azimuthal Integration on GPU. *Powder Diffr.* **2013**, *28*, S339−S350.
(20) Rodriguez-Carvajal, J. Recent Developments of the Program FULLPROF. *Commission on Powder Diffraction (IUCr) Newsletter* **2001**, *26*, 12−19.
(21) Juhas, P.; Davis, T.; Farrow, C.; Billinge, S. J. L. PDFgetX3: a Rapid and Highly Automatable Program for Processing Powder Diffraction Data into Total Scattering Pair Distribution Functions. *J. Appl. Crystallogr.* **2013**, *46*, 560−566.
(22) Farrow, C.; Juhas, P.; Liu, J.; Bryndin, D.; Bozin, E.; Bloch, J.; Proffen, T.; Billinge, S. PDFfit2 and PDFgui: Computer Programs for Studying Nanostructure in Crystals. *J. Phys.: Condens. Matter* **2007**, *19*, 335219−335225.
(23) Neuefeind, J.; Feygenson, M.; Carruth, J.; Hoffmann, R.; Chipley, K. K. The Nanoscale Ordered MAterials Diffractometer NOMAD at the Spallation Neutron Source SNS. *Nucl. Instrum. Methods Phys. Res., Sect. B* **2012**, *287*, 68−75.
(24) Poglitsch, A.; Weber, D. Dynamic disorder in methylammoniumtrihalogenoplumbates (II) observed by millimeter-wave spectroscopy. *J. Chem. Phys.* **1987**, *87*, 6373.
(25) Lee, J. H.; Lee, J.-H.; Kong, E.-H.; Jang, H. M. The Nature of Hydrogen-bonding Interaction in the Prototypic Hybrid Halide Perovskite, tetragonal $CH_3NH_3PbI_3$. *Sci. Rep.* **2016**, *6*, 21687.
(26) Tan, L. Z.; Zheng, F.; Rappe, A. M. Intermolecular Interactions in Hybrid Perovskites Understood from a Combined Density Functional Theory and Effective Hamiltonian Approach. *ACS Energy Lett.* **2017**, *2*, 937−942.
(27) Perdew, J. P.; Burke, K.; Ernzerhof, M. Generalized Gradient Approximation Made Simple. *Phys. Rev. Lett.* **1996**, *77* (18), 3865−3868.
(28) Grimme, S. Semiempirical GGA-Type Density Functional Constructed with a Long-Range Dispersion Correction. *J. Comput. Chem.* **2006**, *27* (10), 1787−1799.
(29) Giannozzi, P.; Baroni, S.; Bonini, N.; Calandra, M.; Car, R.; Cavazzoni, C.; Ceresoli, D.; Chiarotti, G. L.; Cococcioni, M.; Dabo, I.; et al. QUANTUM ESPRESSO: A Modular and Open-Source Software Project for Quantum Simulations of Materials. *J. Phys.: Condens. Matter* **2009**, *21*, 395502.
(30) Rappe, A. M.; Rabe, K. M.; Kaxiras, E.; Joannopoulos, J. D. Optimized Pseudopotentials. *Phys. Rev. B: Condens. Matter Mater. Phys.* **1990**, *41* (2), 1227−1230.
(31) http://opium.sourceforge.net/.
(32) Born, M.; Oppenheimer, R. Zur Quantentheorie der Molekeln. *Ann. Phys.* **1927**, *389*, 457.
(33) Andersen, H. C. Molecular Dynamics Simulations at Constant Pressure and/or Temperature. *J. Chem. Phys.* **1980**, *72* (4), 2384−2393.
(34) Thomas, N. W. The Compositional Dependance of Octahedral Tilting in Orthorhombic and Tetragonal Perovskites. *Acta Crystallogr., Sect. B: Struct. Sci.* **1996**, *52*, 16−31.
(35) Fan, Z.; Xiao, J.; Sun, K.; Chen, L.; Hu, Y.; Ouyang, J.; Ong, K. P.; Zeng, K.; Wang, J. Ferroelectricity of $CH_3NH_3PbI_3$ Perovskite. *J. Phys. Chem. Lett.* **2015**, *6*, 1155−1161.
(36) Ong, P. K.; Goh, T. W.; Xu, Q.; Huan, A. Mechanical Origin of the Structural Phase Transition in Methylammonium Lead Iodide $CH_3NH_3PbI_3$. *J. Phys. Chem. Lett.* **2015**, *6*, 681−685.
(37) Selig, O.; Sadhanala, A.; Mueller, C.; Lovrincic, R.; Chen, Z.; Rezus, Y. L. A.; Frost, J. M.; Jansen, T. L. C.; Bakulin, A. A. Organic Cation Rotation and Immobilization in Pure and Mixed Methylammonium Lead-Halide Perovskites. *J. Am. Chem. Soc.* **2017**, *139*, 4068−4074.
(38) Jodlowski, A. D.; Roldan-Carmona, C.; Grancini, G.; Salado, M.; Ralaiarisoa, M.; Ahmad, S.; Koch, N.; Camacho, L.; de Miguel, G.; Nazeeruddin, M. K. Large Guanidinium Cation Mixed with Methylammonium in Lead Iodide Perovskites for 19% Efficient Solar Cells. *Nature Energy* **2017**, *2*, 972−979.

DOI: 10.1021/acs.jpcc.8b10086
J. Phys. Chem. C 2018, 122, 28265−28272